



HAL
open science

Adsorption of anti-inflammatory and analgesic drugs traces in water on clay minerals

Fatma Mansouri, Khawla Chouchene, Ahmed Wali, Jérôme Labille, Nicolas Roche, Mohamed Ksibi

► **To cite this version:**

Fatma Mansouri, Khawla Chouchene, Ahmed Wali, Jérôme Labille, Nicolas Roche, et al.. Adsorption of anti-inflammatory and analgesic drugs traces in water on clay minerals. *Chemosphere*, 2024, 353, pp.141469. 10.1016/j.chemosphere.2024.141469 . hal-04486562

HAL Id: hal-04486562

<https://amu.hal.science/hal-04486562v1>

Submitted on 14 Jan 2025

HAL is a multi-disciplinary open access archive for the deposit and dissemination of scientific research documents, whether they are published or not. The documents may come from teaching and research institutions in France or abroad, or from public or private research centers.

L'archive ouverte pluridisciplinaire **HAL**, est destinée au dépôt et à la diffusion de documents scientifiques de niveau recherche, publiés ou non, émanant des établissements d'enseignement et de recherche français ou étrangers, des laboratoires publics ou privés.

Adsorption of anti-inflammatory and analgesic drugs traces in water on clay minerals

Fatma Mansouri^{a,c,*}, Khawla Chouchene^b, Ahmed Wali^c, Jerome Labille^d, Nicolas Roche^{d,e}, Mohamed Ksibi^c

^a Higher Institute of Water Sciences and Techniques, University of Gabes, Gabes, 6072, Tunisia

^b Laboratory of Environmental Bioprocesses, Center of Biotechnology of Sfax, University of Sfax, PO 10 Box 1177, 3018, Sfax, Tunisia

^c Laboratory of Environmental Engineering and Ecotechnology, National School of Engineers of Sfax (ENIS), University of Sfax, Route de Soukra Km 3.5, Po. Box 1175, 3038, Sfax, Tunisia

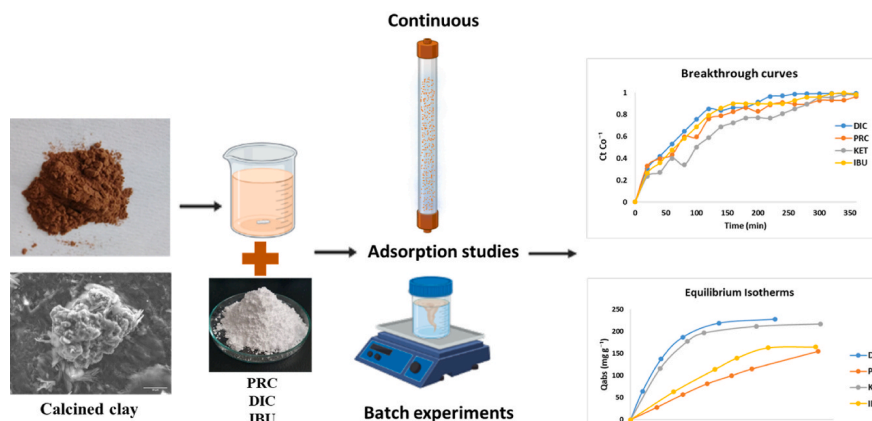
^d Aix-Marseille University, CNRS, IRD, INRAE, Coll France, CEREGE, CEDEX, 13454, Aix-en-Provence, France

^e International Water Research Institute, Mohammed VI Polytechnic University, 43150, Benguerir, Morocco

ARTICLE INFO Handling editor: Vincenzo Naddeo

Keywords: Pharmaceuticals Calcined clay

GRAPHICAL ABSTRACT



ABSTRACT

The aim of this study was to assess the adsorption of four non-steroidal anti-inflammatory drugs (NSAIDs), namely Paracetamol (PRC), Diclofenac (DIC), Ibuprofen (IBU), and Ketoprofen (KET), using both batch and continuous experiments with clay. Various analytical techniques, including XRD, FTIR, SEM coupled to EDX, and Zeta potential, were employed to characterize both raw and calcined clay. XRD and FTIR analyses confirmed the kaolinite nature of the clay. SEM data revealed a lamellar structure formed in the clay after calcination at 550 °C. Adsorption tests were conducted to determine the optimal adsorption conditions. Batch kinetics of adsorption demonstrated rapid adsorption of all four NSAIDs, with the highest adsorption occurring at pH 4 (DIC, IBU, and KET) and pH 6 for PRC, using a concentration of 20 mg L⁻¹ of calcined clay. Additionally, the pseudo-second-order model provided the best fit for all NSAIDs adsorption processes. Maximum adsorption capacities, as determined by the Langmuir model, were 80 mg g⁻¹ for PRC, 238 mg g⁻¹ for DIC, 138 mg g⁻¹ for IBU, and 245 mg g⁻¹ for KET. In fixed bed column studies, three dynamic models (Thomas, Adams-Bohart, and Yoon-Nelson) were utilized to describe the breakthrough curves, with linear regression used to identify key characteristics for process design. The fixed bed column adsorption study revealed that DIC exhibited the highest removal efficiency at 98%, while KET, IBU, and PRC were more persistent, with removal efficiencies of 77.1%, 76.7%, and 67.1%, respectively. The Thomas model was deemed appropriate for describing the breakthrough curve. These findings offer valuable insights into the interactions between clay and pharmaceuticals with varying physicochemical properties. They also provide information on the adsorption models, saturation, and adsorption capacities of various pharmaceuticals on natural clays, which can be crucial for further research and environmental remediation efforts.

Abbreviations: PRC, Paracetamol; DIC, Diclofenac; IBU, Ibuprofen; KET, Ketoprofen; XRD, X-ray Powder Diffraction; FTIR, Fourier-Transform Infrared Spectroscopy; SEM, Scanning Electron Microscope; EDX, Energy-Dispersive X-ray spectroscopy; NSAIDs, Non-Steroidal Anti-Inflammatory Drugs; ZBH, Zeramidine-BNI Hassan; PPs, Pharmaceuticals Products; pKa, Acid dissociation constants; SB, Sugarcane Bagasse; CC, Corn Cobs; BTC, Breakthrough Curve.

* Corresponding author. Higher Institute of Water Sciences and Techniques, University of Gabes, Gabes, 6072, Tunisia.

E-mail address: fatmamansouri93@gmail.com (F. Mansouri).

1. Introduction

Scientific researchers and water treatment operators are currently grappling with the challenge of devising effective solutions for the removal of pharmaceuticals from various environmental sources. This is primarily due to the widespread presence of pharmaceutical residues in environmental compartments. The urgency in finding suitable removal methods arises from the potential ecological and health risks associated with pharmaceuticals, particularly non-steroidal anti-inflammatory drugs (NSAIDs), which can harm aquatic life and human well-being, as documented by (Caban and Stepnowski, 2021; Park et al., 2020). Moreover, the global pharmaceutical industry faced significant impacts from the COVID-19 pandemic, as highlighted by (Ayati et al., 2020). In the context of the pandemic, medications such as ibuprofen “IBU”, ketoprofen “KET” and paracetamol “PRC”, known for their analgesic and antipyretic properties, became pivotal for alleviating COVID-19 symptoms, as emphasized by (Lechien et al., 2020). However, many NSAIDs are not fully metabolized within the human body, leading to their presence in wastewater streams as they exit households and enter sewage treatment facilities. Surprisingly, these pharmaceutical residues often persist in waterways located miles downstream from sewage treatment plants, mainly because many treatment facilities do not routinely eliminate pharmaceutical compounds from the water they process. Regarding the presence and distribution of pharmaceutical compounds such as propranolol, diclofenac “DIC”, and amoxicillin, they have been detected not only in drinking water, as reported by (Thiebault et al., 2019) but also in surface water at concentrations reaching approximately 590 and 158–200 ng L⁻¹, as observed by Maia et al. (2017). These findings have raised concerns regarding the effectiveness of conventional water treatment methods in completely removing these substances. As a result, various wastewater treatment technologies are currently under extensive investigation to prevent the introduction of pharmaceuticals into aquatic environments. These technologies include biological processes like activated sludge, as explored by Nguyen et al. (2021), and membrane bioreactors, as studied by Femina Carolin et al. (2021). Additionally, separation techniques such as nano-filtration and reverse osmosis, as discussed by Al-Jlil (2017), and advanced oxidation processes utilizing ozonation, ultraviolet light, and hydrogen in UV/H₂O₂ processes, as detailed by Baresel et al. (2019), are being actively explored. It’s worth noting that the wide-ranging chemical diversity of pharmaceutical compounds has presented challenges for wastewater treatment technologies when tested at bench-scale levels, as noted by Mansouri et al. (2021). These alternatives can overshadow the use of other treatment process such as calcined clay. Furthermore, implementing these treatments is time-consuming and costly. To meet safe pharmaceutical discharge levels, there is a pressing need for incentives for green technology adoption. In research, there’s a rising emphasis on adsorption, especially using soil like clayey/sandy loam to remove drugs and hormones. Notably, clay, which is abundantly available in numerous countries, has emerged as a prominent tool for these

removal processes, as highlighted by Corbin et al. (2021). Consequently, the utilization of calcined clay as a sorbent has become increasingly valuable. Further exploration of clay’s suitability for the removal of trace pharmaceutical residues from aquatic environments holds significant promise. In this particular investigation, natural clay was procured from the quarry in the Zeramdine-BNI Hassan (ZBH) region of Tunisia. This region is characterized by a juxtaposition of clay and sandy clay patches, as elucidated by Lachaal et al. (2013). Extensive layers of clay constitute the lithostratigraphic formations within the study area, a fact documented by Maalla et al. (2021). The Zeramdine locale in Eastern Tunisia is home to numerous clay quarries, often catering to the needs of various industrial units such as brickworks and ceramics manufacturers. Kaolinite clay, chosen for this study, possesses innate adsorption properties thanks to its layered structure and surface reactivity, rendering it a highly efficient sorbent for pharmaceutical compounds. Opting for raw kaolinite clay preserves its natural adsorption capacity, which could be compromised by chemical alterations. This choice is further justified by the clay’s abundance and wide accessibility, ensuring its suitability for diverse water treatment applications. By employing raw kaolinite clay, we alleviate concerns related to additional processing steps, potential changes to its adsorption characteristics, and the environmental impact associated with modifications. After calcination process, Calcined clay was employed in batch and fixed bed column adsorption experiments aimed at removing three non-steroidal anti-inflammatory drugs (NSAIDs): DIC, IBU, KET, as well as the representative PRC.

This research not only introduces innovation by employing locally sourced or waste-derived supports and materials to create processes with a minimal environmental footprint but also aims to contribute to water treatment. Specifically, the study assesses the adsorption efficiency of calcined clay and explores novel adsorbents for four commonly used pharmaceutical products (PPs). It delves into the impact of operational parameters on adsorption performance, investigates adsorption isotherms and kinetics for a comprehensive understanding, and thoroughly examines and discusses the primary modes of interaction between the adsorbent (clay) and the adsorbate (pharmaceuticals). These materials have proven effective in adsorbing specific molecules and addressing emerging pollutants, emphasizing their significance in sustainable practices.

2. Materials and methods

2.1. Reagents

IBU (CAS 15307-86-5), PRC (CAS 103-90-2) DIC (CAS 15307-86-5) and KET (CAS 22071-15-4) were purchased from Sigma Aldrich (98–99% purity) with pKa values of 4.91; 9.38; 4.15 (Jyoti Sen and Patel, 2016); and 4.4 (Abou-Taleb et al., 2023), respectively. They were used to prepare NSAIDs solutions in various concentrations.

Natural clay (size fraction <63 µm) was collected in the Zeramdine-BNI Hassan (ZBH) area of Monastir governorate, Eastern region of

Tunisia, at longitude and latitude of 35°33'50.69"N and 10°46'54.99"E, respectively (Fig. 1(a)). The Zeramdine sedimentary series is composed primarily of sand and sandy clay interbedded with clay layers from the Saouaf (Serravalian Tortonian) and Segui (Mio-Pliocene) formations (Maalla et al., 2021). Several hundred meters of clays, lignite, sandstones, marls, and sandstones alternating packages of Miocene, Pliocene, and Quaternary make up the lithostratigraphic columns (Maalla et al., 2021).

Samples were crushed and sieved to obtain particle size less than 63 μm through a stainless-steel sieve (RETSCH AS 200). Then before adsorption, the clay sample was calcined at a temperature of 550 °C for 2 h, as described by Garca et al. (2017); Mark et al. (2019) as shown in Fig. 1(b). Therefore, the assessment of the clay's adsorption efficiency and the distinction between natural and calcined clay were accomplished by employing various analytical techniques, with particular emphasis on X-ray diffractometry (XRD).

SEM (HITACHI S-3000 N) coupled to energy dispersive X-ray EDX analysis were used to examine the surface morphology, chemical composition (Oxygen, silicon, aluminum, magnesium), and structure of the adsorbent before and after calcination. X-ray diffraction experiments were carried out using an X-ray diffractometer and XRD-6000, Shimadzu, Kyoto (Japan) using wavelength (λ) 1.5406 Å for CuKα radiation (40 kV and 30 mA), scan range from 10° to 80°, sampling pitch and scan speed was 0.020 and 2 deg min⁻¹ respectively. Infrared spectroscopy using the Fourier transform (FTIR, TENSOR27) was used to record 32 scans with a resolution of 4 cm⁻¹ at room temperature using an attenuated total reflectance (ATR) accessory in diffuse reflectance mode. For zeta potential analysis, a magnetic stirring bar was inserted after a 50 mg sample was put into 50 mL of pure water. Orion electrodes were used to test the pH of the fluid. After adding the clay sample, the pH of the solution was adjusted by adding 0.1 M HCl and NaOH solutions drop by

drop (Yukselen and Kaya, 2003). A Zetasizer Nano ZS (Malvern Instruments, Malvern, England) was used to measure zeta potential for isoelectric titration via pH titration.

2.2. Batch adsorption

In the batch experiment, 100 mL of DIC, PRC, IBU, and KET aqueous solutions were prepared by dilution from concentrated stock solutions (10–80 mg L⁻¹) and placed in a glass flask. PRC and DIC absorbencies were measured using a JENWAY 7315 spectrophotometer at wavelengths of 244 and 277 nm, respectively, and concentrations were estimated using calibration curves (Salaa, 2021; Sulaiman and Al-Jabari, 2021), while IBU and KET were prepared in an alkaline solution (pH = 8) to ensure total dissolution. (0.1 M) HCl or (0.1 M) NaOH was used to adjust the pH of the pharmaceutical solution. The absorbencies of IBU and KET solutions were measured using the same spectrophotometer at wavelengths 220 and 260 nm, respectively (Kerkhoff et al., 2021; Smiljanić et al., 2020). All adsorption experiments were conducted at room temperature (25 ± 0.2 °C). A magnetic stirrer was used to stir 20 mg of calcined clay into the flask during 6 h. At time t₀, the appropriate amount of PPs solution was introduced into the flask and the mixture was kept agitated. At seven time intervals, some aliquots of the batch mixture under agitation were sampled, and centrifuged at 4000 rpm (MIKRO 200) for 10 min. The residual concentration of PPs remaining free in solution in each mixture was then determined using the spectrophotometer at the appropriate wavelength (Fig. 1(c)). Mass balance was used to calculate the amount of pharmaceutical adsorbed on the calcined clay (Q):

$$Q = \frac{(C_0 - C_e) * V}{M} \quad (1)$$



Fig. 1. (a) Localization of clay sample collected from the region of ZBH; (b) Clay adsorbent after calcination at 550 °C; (c) Batch adsorption experiments; (d) Fixed bed column adsorption experiments.

Where Q is the amount of solute retained per mass unit of adsorbent (mg g^{-1}), C_0 and C_e are the initial and equilibrium concentration (mg L^{-1}), M is the amount of sorbent (g), and V is the volume of solution.

The pseudo-first-order kinetics and pseudo-second-order kinetics were used in this study according to Kamatchi et al. (2022). Isotherms including Langmuir (Cundari et al., 2018), Freundlich, (Hidayah et al., 2023) and Temkin models (Sousa et al., 2022) were applied to further investigate the adsorption phenomenon that controls the adsorption of selected pharmaceutical on the surface of calcined clay.

2.3. Fixed bed column

2.3.1. Experimental procedure

A borosilicate glass column with an internal diameter of 16 mm and a total length of 12.5 cm was used for fixed bed experiments. In order to maintain a sufficient hydraulic conductivity, the column was filled with a homogeneous mixture of 90 wt% quartzic sand of 0.5–1 mm grain size and 10 wt% calcined clay. DIC, PRC, KET, and IBU solutions were pre-prepared at 10, 50 and 80 mg L^{-1} in mineral water (Aix les Bains, France). The solutions were pumped up-flow through the column at a flow rate of 0.75 mL min^{-1} during 6 h using a Watson-Marlow Solutions 120S/DV Peristaltic Pump (Fig. 1(d)). All experiments were carried out at 25 °C. A fraction collector was used at the column outlet to recover the percolating solution in 15 mL fractions. The breakthrough curves were obtained by analyzing the effluent fractions with spectrophotometry.

Knowing the cross sectional area A and the flow rate Q , the Darcy velocity V_D is found from the following relationship (Cerepi et al., 2002; Quinn, 2014):

$$VD = \frac{Q}{A}$$

2.3.2. Experimental design

The effects of starting PPs concentration (10, 50, and 80 mg L^{-1}) on adsorbent weight (2 g) and volumetric flow rate were investigated (0.75 mL min^{-1}). In addition, breakthrough curves (BTCs) were obtained by plotting C_t/C_0 as a function of operating time (min) to evaluate pharmaceutical adsorption onto clay under various operational conditions.

The value of the total adsorbed of PPs in the column, qt (mg), can be calculated from the area under the breakthrough curve (Eq. (2)) (Han et al., 2009):

$$qt(\text{mg}) = \frac{Q}{1000} \int_{t=0}^{t=\text{total}} C_{ad} dt = \frac{Q}{1000} \int_{t=0}^{t=\text{total}} (C_0 - C_t) dt \quad (2)$$

Where C_{ad} is the concentration of PPs removal (mg L^{-1}). Equilibrium PPs uptake or maximum capacity of the column, q_{exp} (mg g^{-1}), in the column is calculated as the following:

$$q_{\text{exp}} (\text{mg/g}) = \frac{qt}{m} \quad (3)$$

Where m is the dry weight of the adsorbent in column (g). The total amount of PPs molecules entering the column (mt) is calculated from the following equation:

$$mt = C_0 \frac{Qt_{\text{total}}}{1000} \quad (4)$$

The removal percentage of PPs molecules can be obtained from Eq. (5)

$$\%R = \frac{qt}{mt} * 100 \quad (5)$$

2.3.3. Breakthrough curve modelling

A breakthrough curve mathematical modelling approach has been used to predict the performance of the fixed bed column. Numerous analytical equations have been used to describe the S-shaped curve of

breakthrough. Three models have been employed to characterize the dynamic behavior of the fixed bed column: the Thomas model (Rafati et al., 2019), the Bohart-Adams model (López-Cervantes et al., 2018), and the Yoon-Nelson model (Rafati et al., 2019).

3. Results and discussion

3.1. Adsorbent characterization

3.1.1. XRD

Fig. 2(a and b) depicts the adsorbent's X-ray diffraction pattern. As shown in Fig. 2(a), the major mineral constituents of raw clay are kaolinite and quartz. Fig. 2(b) illustrates the XRD pattern of the calcined clay, characterized by a relative degree of dehydroxylation. After 120 min of thermal treatment at 550 °C, the kaolinite diffraction peaks at 14.2, 24.6, and 50.1°, as well as the less intense peaks at 26.8, 48.0, and 65.1°, disappear, while the quartz peaks (23.01, 50.5, 50.9, and 70.2°) remain unchanged. Mkaouar et al. (2019) demonstrated that kaolinite obtained from the same location as Zeramidine (Jemmel quarry) was converted into metakaolin at temperatures above 450 °C. Metakaolin has been shown to be effective in adsorbing various pollutants, including dyes (Lertcumfu et al., 2018) and heavy metals (Kara et al., 2017). After calcination, the presence of pyrite in the raw clay was transformed to hematite at 38.7°, as revealed by a less intense peak. Furthermore, Liu et al. (2022) reported that pyrite (FeS_2) in coal gangue is transformed into hematite (Fe_2O_3) at temperatures above 600 °C. Al-Hakkani et al. (2022) demonstrate the efficiency of hematite in the removal of Cefixime in pharmaceutical wastewater, with a maximum adsorption capacity of 147.1 mg g^{-1} .

3.1.2. FTIR

The FTIR spectroscopy results of raw clay (Fig. 2(c)) show the kaolinite characteristic bands. Tironi et al. (2012) discovered that kaolinite has absorption bands corresponding to the stretching frequencies of OH groups between 3500 and 3750 cm^{-1} . They are visible as the thin bands at 3619 cm^{-1} and 3695 cm^{-1} characterizing the raw clay. In addition, the following absorption bands are identified: Al–OH at 910 cm^{-1} , Si–O at 1003, and Si–O–Al at 777 cm^{-1} and 795 cm^{-1} . Fig. 2(c) demonstrates that the calcined clay lacks a detectable Al–O–H band at 910 cm^{-1} and the doublets at 3619 and 3695 cm^{-1} , indicating that the kaolinite was transformed into metakaolinite, as reported by Kassa et al. (2022), which confirms the XRD results. The band's absence at 910 cm^{-1} can be attributed to the OH deformation of inner hydroxyl groups (Bukalo et al., 2017). The band at 1089 cm^{-1} is assigned to amorphous SiO_2 . The deformation vibrations of –OH were justified by the reduced intensity of diffusing bands observed at 1633–1651 cm^{-1} .

3.1.3. SEM- scanning electron microscopy with energy-dispersive X-ray spectroscopy (SEM-EDX)

Fig. 2(e and f) depicts the textural characteristics of clay samples obtained through SEM analysis. SEM images show that the samples have a discontinuous structure and an open texture, with visible and connected voids. Calcined clay has a compacted microstructure with a porous structure, which can provide a high porosity value and high adsorption capacity, as shown in Fig. 2(f), which has a higher coarse fraction than natural clay. The EDX analysis measurements for both raw and calcined clay are shown in Fig. 2(e and f). Natural clay's chemical composition revealed that it contained a high concentration of O, Si^{4+} and Al^{3+} oxides and exchangeable interlayer cations such as Na^+ , Mg^{2+} , Ca^{2+} , K^+ , and Fe^{3+} . Si, Al and O are kaolin constituents. Similarly, the major components discovered for calcined clay were O, Al, and Si, with percentage wt% values of 72.84, 8.33, and 13.70 respectively. EDX confirms the XRD analysis results for transforming pyrite to hematite after calcination with the loss of sulfur.

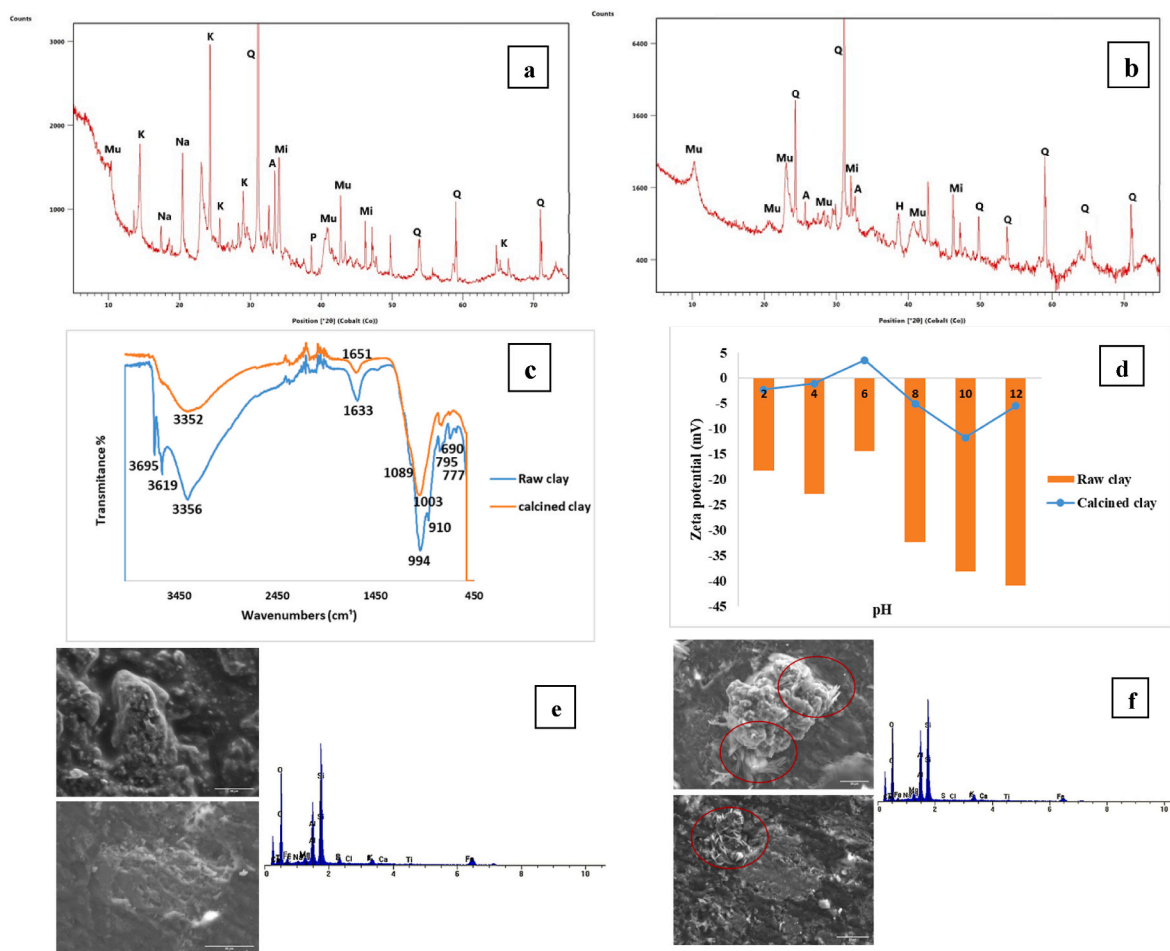


Fig. 2. Characterization of raw and calcined clay (a: XRD analysis for raw kaolinite; b: XRD analysis calcined clay; c: FTIR; d: Zeta potential; e: SEM-EDX analysis for raw clay; f: SEM-EDX analysis for calcined clay).

3.1.4. Zeta potential

Measurements of varying pH (Fig. 2(d)) revealed that the raw clay has a negative charge for natural clay across all pH ranges. The zeta potential in our study ranged from -20.4 mV to -40.9 mV. According to [Yukselen and Kaya \(2003\)](#), the zeta potential of kaolinite in water ranged from -25 mV (pH 3) to -42 mV (pH 11). The negative zeta potential values of natural kaolinite clay can be supported by the fact that kaolinite clay particles comprise a permanent negative charge arising from the isomorphous substitution of structural Si^{4+} by Al^{3+} , whereas the zeta potential variation measured from pH 2 to pH 11 can be attributed to the additional contribution of the OH groups with a pH-dependent charge at the edges of the kaolinite clay particles. In contrast, calcined clay has a weak positive charge of 3.56 mV at pH = 6. The adsorbent efficacy largely depends on its surface charge, indicating its surface's acidic or basic character ([Chauhan et al., 2020a](#); [Kumari and Mohan, 2021](#)). The isoelectric point of the sheet edges of the calcined clay is probably close to pH = 7. Therefore, at pH < 7, the edge surface tends to be positively charged, but the structural charge remains unchanged and the overall clay charge remains negative. The negative charge is logically more pronounced at pH > 7, as the edge surface tends to be negatively charged ([Sousa et al., 2022](#)). Nevertheless, it is worthwhile noting that the surface charge amplitude of the clay is strongly decreased after calcination. This can be associated to the dihydroxylation reaction observed with XRD and FTIR. IBU, DIC, KET, and PRC have pKa values of 4.91, 4.51, 4.4, and 9.38, respectively. At pH < 4, the surface charge of IBU, DIC, and KET is neutral as their reactive moieties are protonated, and PRC has a neutral charge at pH < 9. Therefore, we expect that for pH < pKa, the maximum amount of PPs

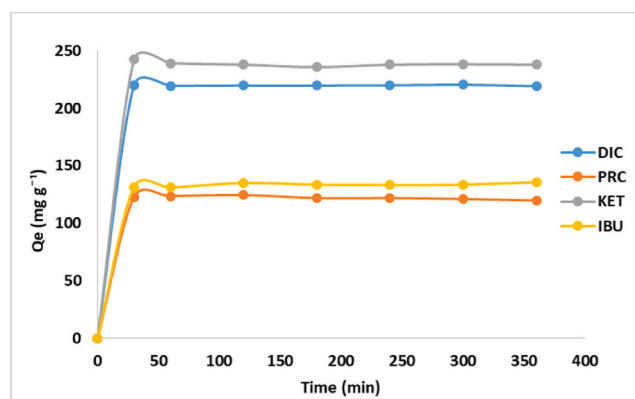
is adsorbed onto the clay through hydrophobic interactions, while at pH > pKa, electrostatic repulsions might limit the adsorption. Meanwhile, considering the low surface charge of the calcined clay, electrostatic interactions might not be the driving parameter and adsorption could still take place at pH > pKa.

3.2. Batch adsorption

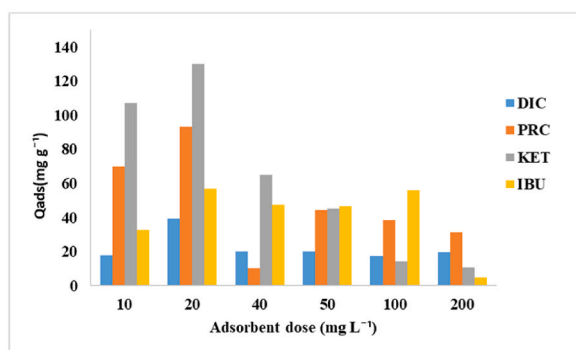
3.2.1. Effect of contact time

Fig. 3(a) presents pharmaceuticals removal at different contact times examined at clay concentration of 20 mg L^{-1} for DIC, PRC, KET, and IBU. Pharmaceuticals removal increased rapidly with the increase of contact time, but after 20–30 min, started constant value denoting the attainment of equilibrium. Indeed, it can be observed from Fig. 3(a) that the fast adsorption of pharmaceutical products and maximal retention is reached after the initial first hour. This is due to the presence of vacant and abundant active sites on the adsorbent which became used up saturated with time by attaining equilibrium ([Khazri et al., 2017](#); [Smiljanić et al., 2020](#); [Streit et al., 2021](#)). After 120 min of contact time, no significant change in the adsorbed drug levels was observed, indicating that the adsorption process had reached an equilibrium state. At this juncture, it was evident that the available sorption sites on the calcined clay were effectively saturated, as also noted by [Khazri et al. \(2017\)](#).

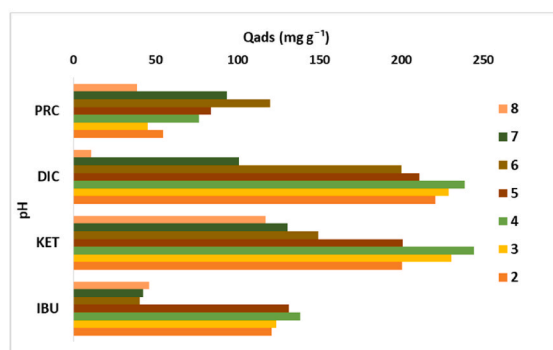
These results support similar behavior on clay as per adsorption of IBU and PRC, mentioned by [Khazri et al. \(2017\)](#) and [Corbin et al. \(2021\)](#), respectively. Also, [Streit et al. \(2021\)](#) noted that the adsorption rate of KET and DIC gradually decreased, and equilibrium was attained at 180



(a)



(b)



(c)

Fig. 3. (a) Effect of contact time on adsorption of PRC, DIC, IBU and KET using clay adsorbent ($T = 25\text{ }^{\circ}\text{C}$; $C_0 = 50\text{ mg L}^{-1}$; Concentration of adsorbent = 20 mg L^{-1}); (b) Effect of varying concentration dose of clay; (c) Effect of pH on the removal of IBU, KET, DIC and PRC using calcined clay adsorbent ($T = 25\text{ }^{\circ}\text{C}$; $C_0 = 50\text{ mg L}^{-1}$; $t = 2\text{ h}$; Concentration of adsorbent = 20 mg L^{-1}).

min. This suggests that a more rapid equilibrium is obtained in this study. Meanwhile, in spite of this higher adsorption kinetics, different affinities between the adsorbent and adsorbate apparently take place depending on the pharmaceutical molecule, as suggested by the Q_t values ranging from 120 mg g^{-1} for PRC to 238 mg g^{-1} for KET. In a comparable experimental setup to our study, [Streit et al. \(2021\)](#) documented reduced adsorption capacities as follows: 85 mg g^{-1} for IBU, 40 mg g^{-1} for KET, and 50 mg g^{-1} for PRC, all observed at an initial concentration of pharmaceutical products of 50 mg L^{-1} . In their study, [Nourmoradi et al. \(2018\)](#) found that optimal adsorption occurred within 120 min for IBU and 150 min for PRC when utilizing activated carbon as the adsorbent material. The sorption capacities for PRC and IBU were evaluated to be 36.52 mg g^{-1} and 35.49 mg g^{-1} , respectively.

3.2.2. Adsorption kinetics modelling

The kinetic parameters of pharmaceuticals adsorption onto clay at various contact times were investigated. [Table 1\(a\)](#) displays all of the kinetic parameters for the adsorption of the four pharmaceuticals. The results showed that the pseudo-first-order equation poorly fits all of the pharmaceuticals experimental data. This is indicated by their low linear regression (R^2) values, which are not close to 1. Moreover, the calculated adsorption capacities Q_{cal} values were far lower than the experimental values. The pseudo-second-order kinetic model provided the best fit, with R^2 values of 0.9997, 0.9999, 0.9997, and 0.9995 for PRC, DIC, IBU, and KET, respectively.

Furthermore, the Q_{cal} values calculated using the pseudo-second-order model are very close to the experimentally determined values ([Fig. 4\(b\)](#)). This model assumes that chemisorption is the primary process of pharmaceutical adsorption onto calcined clay. Similarly,

Table 1a

Kinetic parameters and isotherms for the four pharmaceuticals products onto clay adsorption.

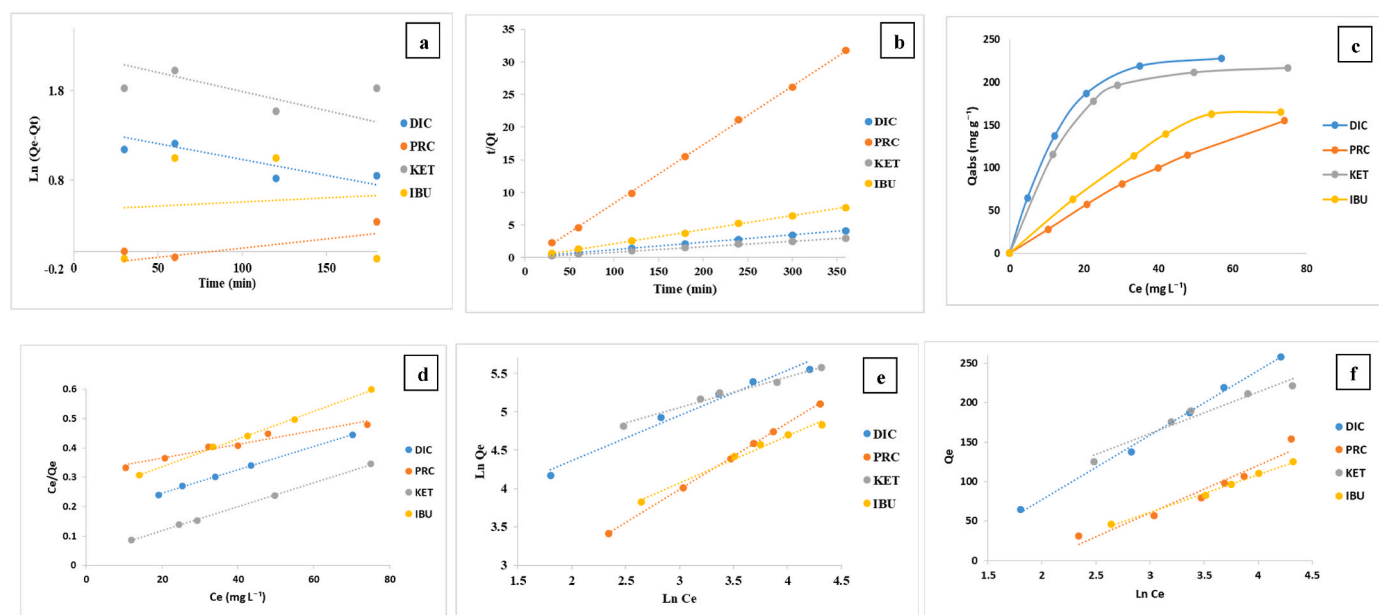
	PRC	DIC	IBU	KET
First-pseudo order				
$Q_{exp}\text{ (mg g}^{-1}\text{)}$	13	87.20	63	121
$Q_{cal}\text{ (mg g}^{-1}\text{)}$	0.847	3.990	1.457	9.204
$K_1\text{ (min}^{-1}\text{)}$	0.002	0.0035	0.0017	0.0043
R^2	0.7063	0.7987	0.1489	0.7798
Second-pseudo order				
$Q_{exp}\text{ (mg g}^{-1}\text{)}$	13	87.20	63	121
$Q_{cal}\text{ (mg g}^{-1}\text{)}$	11.123	86.956	63.291	120.481
$K_2\text{ (g}^{-1}\text{ mg}^{-1}\text{ min}^{-1}\text{)}$	-0.0059	0.0028	-0.0072	0.0014
R^2	0.9997	0.9999	0.9997	0.9995
Langmuir				
$Q_m\text{ (mg g}^{-1}\text{)}$	434.782	370.37	250	243.902
$K_L\text{ (L mg}^{-1}\text{)}$	0.0016	0.002	0.003	0.004
R^2	0.9516	0.9993	0.9994	0.9995
Freundlich				
n_f	1.155	1.875	1.429	2.493
K_F	4.004	24.143	9.325	47.153
R^2	0.9999	0.9759	0.9411	0.9833
Temkin				
b_T	41.162	30.370	32.963	46.865
K_T	0.136	0.348	0.1411	1.046
R^2	0.9444	0.9961	0.964	0.9549

[Chauhan et al. \(2020b\)](#) showed that the adsorption of amoxicillin, PRC, imipramine (IMP), and DIC using Ti-pillared montmorillonite clay also follows closely the pseudo-second-order kinetic mode, and [Streit et al. \(2021\)](#) came to the same observation by using activated carbon for the

Table 1b

Fixed bed column performance parameters and Thomas, Yoon-Nelson and Adams-Bohart models for PPs adsorption onto calcined clay.

Parameters	PRC			DIC			IBU			KET		
$Q_{e \text{ exp}}^*$ (mg g ⁻¹)	5.243			5.434			5.186			5.354		
Q_e^* (mg)	2.621			2.717			2.593			2.677		
W_{total}^* (mg)	6.832			5.452			6.719			7.976		
%Removal*	67.12			98			76.74			77.18		
Co (mg L ⁻¹)	10	50	80	10	50	80	10	50	80	10	50	80
Thomas												
$Q_{o \text{ cal}}$ (mg g ⁻¹)	1.186	5.637	8.154	1.1595	5.34	8.090	1.863	5.315	8.166	1.182	5.385	8.217
K_{TH} (L min ⁻¹ mg ⁻¹)	0.54	0.052	1.38	0.63	0.068	0.030	0.17	0.142	0.019	0.86	0.1	1.351
R ²	0.953	0.942	0.923	0.961	0.904	0.911	0.971	0.964	0.912	0.985	0.975	0.932
Yoon-Nelson												
τ (min)	121.187	42.238	58.249	134.772	75.65	30.125	239.589	32.601	61.920	179.7	97.344	66.048
K_{YN} (L mg ⁻¹ min ⁻¹)	0.008	0.0105	0.0253	0.008	0.016	0.002	0.008	0.013	0.034	0.008	0.012	0.023
R ²	0.964	0.941	0.911	0.962	0.855	0.884	0.964	0.959	0.839	0.977	0.959	0.814
Adams-Bohart												
N_0 (mg L ⁻¹)	0.590	2.681	3.836	0.586	15.75	41.889	4.056	15.246	23.069	3.865	16.610	23.590
K_{AB} (L mg ⁻¹ min ⁻¹)	0.3	0.038	0.0213	0.33	0.048	0.02	0.46	0.038	0.016	0.38	0.06	0.021
R ²	0.946	0.956	0.906	0.971	0.952	0.884	0.931	0.866	0.9	0.959	0.963	0.915

* Fixed bed column performance in PPs removal at initial concentration of 50 mg L⁻¹**Fig. 4.** (a) Pseudo- First-Order models; (b) Pseudo-Second order models of adsorption PPs; (c) Equilibrium isotherms of DIC, IBU, and KET (pH = 4) and PRC (pH = 6) on clay (T = 25 °C; t = 120 min; C₀ = 0–80 mg L⁻¹; Concentration of adsorbent = 20 mg L⁻¹) and adsorption isotherms (d; Langmuir, e; Freundlich, f; Temkin for adsorption time = 120 min).

removal of PRC, IBU, and KET.

3.2.3. Adsorbent dose

Equilibrium studies were performed to analyze the performance of the adsorbent. The data were generated by varying the adsorbent dose (10–200 mg L⁻¹) at room temperature.

Fig. 3(b) depicts a bird's-eye view of how higher clay concentration generally tends to reduce the amount of pharmaceutical adsorbed per mass of clay. Li et al. (2013); Padmavathy et al. (2016) reported similar findings. The observed pattern can be elucidated by the escalated adsorbent dosage, which leads to a higher abundance of active adsorption sites available for pharmaceutical molecules. This phenomenon highlights the direct relationship between the amount of adsorbent used and the increased capacity to adsorb pharmaceutical compounds. Romdhani et al. (2023). Across all concentrations of DIC, PRC, KET, and IBU, the adsorption process reaches equilibrium within 120 min, with the most pronounced adsorption capacity observed at a dosage of 20 mg L⁻¹ of calcined clay. This phenomenon can be attributed to the

substantial presence of readily available, unoccupied adsorbent sites, which expedite adsorption from the very onset of the process. This highlights the efficiency of the adsorbent and its capacity to swiftly interact with the targeted pharmaceutical compounds (Azari et al., 2022). However, along with adsorption going on, the remaining sites become fewer and less accessible due to repulsive forces between the pharmaceutical molecules on the surface and the un-adsorbed pharmaceutical molecules, as well as the adsorbent's structure (Tatarchuk et al., 2023). The maximum adsorption observed at a dosage of 20 mg per L of calcined clay indicates an optimal equilibrium between various factors. In this context, a harmonious balance exists between the quantity of available adsorption sites and the effectiveness of diffusion mechanisms. This equilibrium implies that the calcination process inherently boosts the clay's hydrophobicity (Chandrasekhar and Ramaswamy, 2002; Wahyuni et al., 2023), resulting in a significantly enhanced sorption capacity for these four products. Hydrophobicity is created during calcination and the surface chemistry becomes more compatible with organic compounds (Souza et al., 2022). Furthermore,

Ewis et al. (2022) demonstrated a notable improvement in the diffusion rate of molecules within the calcined clay matrix. This harmonious balance between increased hydrophobicity, enhanced sorption capacity, and efficient diffusion mechanisms highlights the favorable impact of the calcination process on clay's adsorption and transport properties.

3.2.4. Effect of pH

Fig. 3(c) depicts the effect of pH on pharmaceutical removal by the calcined clay. When the pH was changed from 4 to 8, the removal of IBU, DIC, and KET decreased progressively. IBU, DIC, and KET adsorption capacities decreased from 138 to 46 mg g⁻¹, 238 to 10 mg g⁻¹, and 245 to 117 mg g⁻¹, respectively. Furthermore, the most significant adsorption occurred at pH = 4. Similar results for IBU adsorption by natural clay at pH = 3 have been reported (Khazri et al., 2017). However, at pH

= 6, the adsorption rate for PRC increased, with an adsorption capacity ranging from 120 to 38 mg g⁻¹. The effect of pH can be explained by the different interactions between drugs and clay in terms of surface charge and degree of interaction (Sousa et al., 2022). When the charges of the adsorbate molecules and the adsorbent surface are opposite, attractive electrostatic forces tend to exist, which can aid in the adsorption process. Electrostatic attraction forces can explain these findings. IBU, DIC, and KET have pKa values of 4.91, 4.15, and 4.4, respectively. That means that the three pharmaceuticals have a nearly neutral charge at pH 4. The surface of calcined clay is weakly positively charged because the pH_{pzc} is less than 7. The high adsorption capacity at pH < pKa is probably due to some hydrophobic attractions between pharmaceutical products and the calcined clay. As a result, in the pH range of 4–8, the removal efficacy of the three tested compounds decreased. However, different sensibilities are observed among the three molecules. The lowest pH sensitivity is obtained with KET, which is still removed at 117 mg g⁻¹ at pH = 8, giving a removal twice as low as at pH = 4. To the opposite, the sharpest pH effect is obtained with IBU, as the removal drops from 138 down to <50 mg g⁻¹ as soon as the pH reaches the pKa value. Finally, DIC removal by the clay displays a stronger but more progressive pH effect, decreasing from 240 to 10 mg g⁻¹. It is a polar molecule that has two bulky chlorine atoms. For adsorption, the volume of the molecule must also be considered, as well as whether it can fit into the cavities of the adsorbent. Because of pKa = 4.15, at pH = 7–8, deprotonation of the -COOH group to -COO⁻ occurs, making the molecule negatively charged and tending to reject the adsorbent's surface charge. At pH 4, the sorption efficiency on calcined clay was quite high, when deprotonation did not occur, same results have been shown by Szabová et al. (2022). The adsorption rate of PRC was shown to be lower at pH > 6. That may be attributed to the repulsion between the negative surface charges of clay and the PRC molecules progressively deprotonating when pH gets closer to the pKa (9.38) (Ferreira et al., 2015). However, in basic solutions, PRC molecules have a significantly larger charge density that is repelled by the negatively charged sample. In this instance, physorption may be more important. The removal percentage of DIC with almost 98% is higher than KET (34%) > IBU (32%) at pH = 4 > PRC (16%; pH = 6).

3.2.5. Adsorption isotherms

Data from adsorption isotherms starting at various initial concentrations of DIC, IBU, PRC, and KET were investigated. These results were obtained by measuring drug concentrations after pharmaceutical/clay contact times equal to the equilibrium times. As a result, all drugs' adsorption isotherms are plotted in Fig. 4(c). According to the data, the adsorption capacities of DIC (Q_e = 228 mg g⁻¹) and KET (Q_e = 217 mg g⁻¹) were greater than that of IBU (Q_e = 163 mg g⁻¹) and PRC (Q_e = 150 mg g⁻¹).

Additionally, it appears that the DIC, KET, and IBU adsorption kinetic curves on calcined clay are all characterized by a similar adsorption dynamic (Fig. 4(c)). The curve shapes for these three pharmaceuticals are type L2, indicating that the active sites of adsorption have been saturated and exhausted (Streit et al., 2021). Even at low

initial concentrations, the calcined clay has a high affinity for these three drugs. In contrast, the PRC curve did not have a plateau (Streit et al., 2021), which could indicate that the active sites of the clay adsorbent were not fully occupied. According to the isotherm classification proposed by Giles et al. (1960), this type of curve is generally related to type L1.

The linearized form was used to determine the Langmuir, Freundlich, and Temkin isotherm parameters, and their values, along with the respective correlation coefficients, are listed in Table 1(a). The Langmuir isotherm fits the equilibrium data with the highest accuracy among the linear models under our experimental conditions. However, the difference was minor when compared to the Freundlich model. As a result, it is unclear whether adsorption occurred on a homogeneous or heterogeneous surface. Furthermore, the Langmuir model assumes monolayer adsorption. In contrast, the Temkin isotherm model (Fig. 4(f)) assumes that the adsorption heat of all molecules decreases linearly with the increase in coverage of the adsorbent surface. That adsorption is characterized by a uniform distribution of binding energies up to a maximum binding energy.

Data in Table 1(a) shows that the best correlation coefficients were, in decreasing order, Langmuir > Temkin > Freundlich models. The highest value of R² for calcined clay was fitted to the Langmuir model (Fig. 4(d)). Fig. 4(d) shows the fit of experimental data with the linearized form of the Langmuir isotherm model. The isotherm parameters calculated of PPs in this study agreed with the data reported by Ayawei et al. (2017); Khazri et al. (2017) and Wang and Guo (2020). This finding may explain the monolayer coverage on the outer surface, which is characterized by uniform functional site occupation by DIC, IBU, and KET, and assumes an entire site interaction between the three NSAIDs and calcined clay. But the adsorption capacity at the plateau for IBU is lower than for DIC and KET. This may suggest that some sites used for DIC and KET are not enough energetic for IBU adsorption, which is not compatible with Langmuir model. A second hypothesis is that IBU having a slightly smaller molecular weight than DIC or KET, even if the same number of molecule is absorbed for the three candidates, in term of mass this results in a lower amount adsorbed for the smaller molecule. However, if the energy of interaction was the same for the three molecules, the isotherm slope would be similar. This makes us think that the first hypothesis is more likely.

Furthermore, as shown in Fig. 4(e) the Freundlich model best fits PRC adsorption. The calculated coefficient was less fitting to the experimental data, excluding the possibility of non-uniform adsorption of PRC onto a heterogeneous surface, which is consistent with the data reported by Elamin et al. (2021) and Kryuchkova et al. (2021).

3.3. Fixed bed column adsorption

3.3.1. Breakthrough analysis

The breakthrough curve measured with the fixed bed column system are presented in Fig. 5. The effect of initial PPs concentration was studied here using the same clay as for batch adsorption. According to flow rate value, the superficial velocity in Darcy equation is equal to 1.041 m s⁻¹. Lee et al. (2023) demonstrated that for the removal of Methylene Blue in a sand-illite mixture, there is no effect of Darcy's velocity values on the breakthrough behavior. Results from Fig. 5 and Table 1(b) show that the fraction of PPs retained by the clay decreases as the initial inlet concentration increases. Fig. 5 demonstrates that when the PPs concentration increased from 10 to 80 mg L⁻¹, the aqueous solution reached the breakthrough point faster. The aqueous solution reached the breakthrough point of DIC, PRC, KET, and IBU 70 min, 180 min, 120 min, and 140 min earlier at 80 mg L⁻¹, when compared to 50. This might be because a larger PPs influent concentration increased the driving force for mass transfer across the liquid film and accelerated the adsorption rate, resulting in earlier exhaustion of the fixed-bed column (Yanyan et al., 2018). Breakthrough curves were dispersed throughout the elution time at lower inlet concentrations (10 mg L⁻¹), as seen by

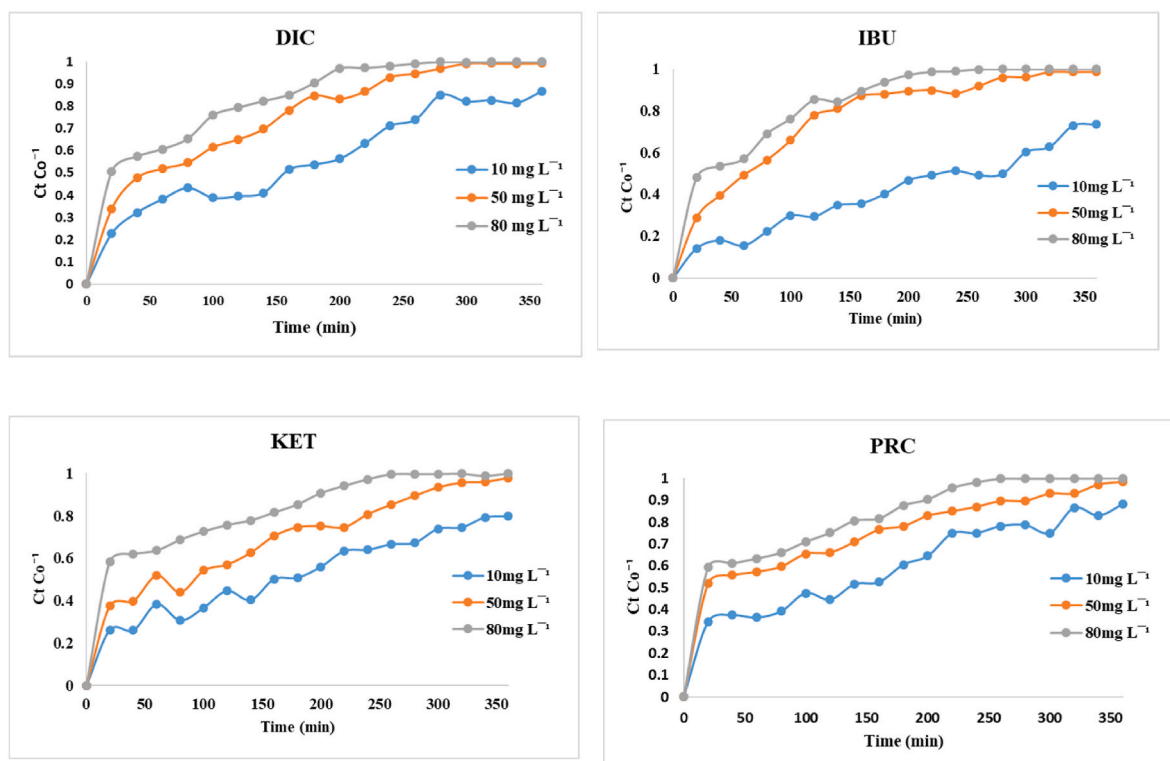


Fig. 5. Breakthrough curves of PPs fixed-bed column adsorption onto calcined clay as function of: $Q = 0.75 \text{ mL min}^{-1}$; $Z = 12.5 \text{ cm}$.

López-Cervantes et al. (2018). When the BTC reaches 1, this means that the sorbent does not retain anymore the NSAIDs. This is clearly seen as a progressive trend here for the four NSAIDs molecules, with a more rapid breakthrough when the inlet solution is more concentrated in PPs, i.e. the sorbent saturation takes place more rapidly. This can be explained by the fact that a low influent concentration causes a slow transport of the PPs to the surface of the calcined clay adsorbent. The removal percentage of DIC with almost 98% is higher than KET (77%) > IBU (76%) > PRC (67%).

It is proposed that the absorption of PPs from the liquid phase to the solid surface occurs via mass transfer as adsorption of PPs at adsorbent interior sites and intraparticle diffusion of PPs or its species within adsorbent pores.

3.3.2. Mathematical modelling

3.3.2.1. Thomas model. Based on the Thomas model, the Thomas kinetic coefficient (K_{Th}) and the maximum solid phase concentration Q_0 (mg g^{-1}) were calculated, and results are grouped in Table 1(b). The R^2 of the plots ranges from 0.913 to 0.942, 0.904 to 0.921, 0.891 to 0.971, and 0.915 to 0.932 for PRC, DIC, IBU, and KET, respectively, suggesting that the Thomas model adequately fits all PPs concentrations. Table 1(b) shows that the calcined clay's adsorption capacity (Q_0) increased with increasing the PPs concentration in the inlet solution, while the value of K_{th} decreased. The experimental $q_{0,exp}$ and calculated $q_{0,cal}$ (Table 1(b)) values did not differ significantly, showing that the simulated experimental data fit the Thomas model well.

3.3.2.2. Adams-Bohart model. The Bohart-Adams model is frequently used to describe the initial behavior of the breakthrough curve. K_{AB} kinetic constant values were higher for lower C_0 (10 mg L^{-1}), while the adsorption capacity N_0 was lower (Table 1(b)). This characteristic is related to the kinetics of adsorption. The drop in K_{AB} found at high C_0 (80 mg L^{-1}) values implies that the overall system kinetics is regulated by external mass transfer in the early stages of fixed bed column

adsorption (de Franco et al., 2018). The correlation coefficient R^2 of initial concentration 10 mg L^{-1} of all PPs ranges from 0.931 to 0.971.

3.3.2.3. Yoon-Nelson model. The Yoon-Nelson model is suitable for single-component systems. The parameters of this model are listed in Table 1(b). All PPs had the longest 50% breakthrough time at 10 mg L^{-1} : 239.5, 134.7, 121.1, and 179.7 min for IBU, DIC, PRC, and KET, respectively. Yoon-Nelson rate constant K_{YN} increases with the increasing of initial PPs concentration. The saturation of the fixed bed column occurred earlier when its initial concentration was higher. Correlation coefficients related to experimental and predictable data using the Yoon-Nelson model in all phases ranged from 0.814 to 0.977.

3.4. Comparison batch and fixed bed column adsorption through isotherm parameters

Tables 1(a) and 1(b) show isotherm parameters, and values for batch (Langmuir, Freundlich, and Temkin) and fixed bed column (Thomas, Adams-Bohart, and Yoon-Nelson) experiments. Table 1(a) shows that higher correlation coefficients (R^2), closer to one, as represented by the Langmuir model, indicate that is the most applicable. In the batch isotherm, values of Langmuir affinity constant (K_L) less than 1 indicate a strong interaction between adsorbate and adsorbent, and Freundlich sorption intensity (n) is greater than 1, confirming the represented favorable adsorption conditions. Tables 1(a) and 1(b) compare the maximum adsorption capacity-related to the Langmuir and Thomas isotherms for NSAIDs removal onto calcined clay in batch and fixed bed column studies. PRC was shown to be better adsorbed in batch experiment (434.7 mg g^{-1}), whereas in fixed bed column study only 5.6 mg g^{-1} was achieved.

4. Comparison with other studies

The removal capacity of calcined clay exhibits a remarkable improvement at a dosage of 20 mg L^{-1} . Equilibrium in adsorption was

Table 2
Comparative analysis of calcined clay adsorbent performance against prior research.

PPs	Adsorbent	pH	T °C	Qmax (mg g ⁻¹)	Literature
Batch adsorption					
IBU	Na-clay	6	25 (±0.2 °C)	36.0	Khazri et al. (2017)
	Calcined clay	4		138	This study
DIC	Montmorillonite	7		2.53	Chauhan et al. (2020b)
	Clay-pillared with titanium oxide	7		23.05	
	Natural Bentonite	5.4		62.5	Mabrouki and Akretche (2016)
	Na-Bentonite	5.4		40.0	
	Iron-pillared Bentonite	5.4		100	
PRC	Calcined clay	4		238	This study
	Montmorillonite	7		3.99	Chauhan et al. (2020b)
	Calcined clay	6		120	This study
Adsorption in a fixed bed column					
PRC	Sugarcane Bagasse (SB)	6	25 (±0.2 °C)	0.32	Juella (2020)
	Corn cob (CC)			0.47	
	Calcined clay	7		5.63	This study
IBU	Nano-clay-composite based on cloisite 15A	7–8		5.60	Rafati et al. (2019)
	Calcined clay	7		5.31	This study

achieved within 120 min for all the pharmaceutical products examined in this study.

As indicated in Table 2, Khazri et al. (2017) employed a dosage of 1 kg of Na-clay per liter, comprising a blend of smectite-kaolinite clay sourced from Jbel Sejnane in northeastern Tunisia, for the adsorption of IBU. They reached equilibrium after 240 min, achieving a maximum adsorption capacity of 36 mg g⁻¹. In contrast, our study achieved a significantly higher maximum adsorption capacity of 138 mg g⁻¹ using calcined clay at a dosage of only 20 mg L⁻¹. This highlights the efficient utilization of calcined clay, resulting in an enhanced adsorption capacity even at lower adsorbent dosages and shorter contact times.

In the study conducted by Mabrouki and Akretche (2016), batch adsorption was utilized to eliminate DIC using bentonite clay sourced from Algeria. The results showed a maximum adsorption capacity of 62.5 mg g⁻¹ at a pH of 5.4, as displayed in Table 2. In contrast, our calcined clay demonstrated a notably superior adsorption capacity, exceeding 230 mg g⁻¹ at pH 4.

Chauhan et al. (2020b) explored the removal of PRC by employing unaltered montmorillonite clay sourced from India, resulting in a relatively modest adsorption capacity of 3.99 mg g⁻¹ within a 60 min contact time. In contrast, in our study, calcined clay exhibited a markedly higher adsorption capacity of 120 mg g⁻¹.

In the context of removing PRC by fixed-bed column, Juella (2020) conducted experiments with two distinct adsorbents, sugarcane bagasse (SB) and corn cobs (CC), as detailed in Table 2. These investigations yielded significantly low adsorption capacities of 0.32 mg g⁻¹ for SB and 0.47 mg g⁻¹ for CC. However, when employing the calcined clay under study for fixed bed column adsorption, a substantial enhancement in adsorption capacity was observed, reaching 5 mg g⁻¹ for the efficient removal of PRC.

Furthermore, Rafati et al. (2019) utilized a Nano-clay composite that included cloisite 15A for the removal of IBU. Their study yielded results nearly identical to ours, demonstrating an adsorption capacity exceeding 5 mg g⁻¹.

5. Conclusion

Clay adsorbent from the geographical location ZBH quarry was used. The presence of kaolinite as the dominant mineral phase in the clay sample, along with alumino-silicate and quartz, was revealed by mineralogical analysis. Batch experiments and fixed bed column adsorption were carried out to investigate the removal of DIC, PRC, KET, and IBU using this calcined clay. Several sorption factors, such as adsorbent dosage, contact time, pH effect, and initial PPs concentration, were investigated to improve the reaction conditions for the adsorption process. The batch adsorption study revealed that the process followed

the Langmuir isothermal model for DIC, IBU, and KET and the Freundlich model for PRC. For DIC, IBU, KET, and PRC, the maximum adsorption capacities of the formed monolayers were found to be 238, 138, 245, and 80 mg g⁻¹, respectively. On the other hand, the kinetic studies confirmed that the adsorption path fit the pseudo-second-order kinetic model. A fixed bed column adsorption study was carried out to investigate the removal efficiency of calcined clay under continuous flow-through and at various PPs concentrations. The Thomas model appeared to be suitable for describing the breakthrough curves. Calcined clay is thought to be the most effective adsorbent using fixed-bed adsorption removal material with a percentage of removal for DIC (98%), KET (77%), IBU (76%), and PRC (67%). This study highlights the potential of calcined clay as a cost-effective, efficient, and eco-friendly adsorbent for treating wastewater contaminated with pharmaceutical residues. By combining clay with sand in specific ratios and subjecting it to solar radiation, the adsorbed molecules undergo degradation via solar photocatalysis. However, it's crucial to emphasize that while this concept shows promise, its practicality and effectiveness require validation through rigorous scientific research and pilot-scale testing.

CRedit authorship contribution statement

Fatma Mansouri: Data curation, Methodology, Investigation, Writing – original draft. **Khawla Chouchene:** Resources. **Ahmed Wali:** Methodology, Investigation. **Jerome Labille:** Validation, Writing – review & editing. **Nicolas Roche:** Formal analysis, Supervision, Writing – review & editing. **Mohamed Ksibi:** Conceptualization, Formal analysis, Investigation, Resources, Supervision, Validation, Writing – review & editing.

Declaration of competing interest

The authors declare that they have no known competing financial interests or personal relationships that could have appeared to influence the work reported in this paper.

Data availability

Data will be made available on request.

References

- Abou-Taleb, H.A., Shoman, M.E., Makram, T.S., Abdel-Aleem, J.A., Abdelkader, H., 2023. Exploration of the safety and Solubilization, dissolution, analgesic effects of common basic excipients on the NSAID drug ketoprofen. *Pharmaceutics* 15, 713. <https://doi.org/10.3390/pharmaceutics15020713>.
- Al-Hakkani, M.F., Gouda, G.A., Hassan, S.H.A., Mohamed, M.M.A., Naguib, A.M., 2022. Cefixime wastewater management via bioengineered Hematite nanoparticles and the

- in-vitro synergetic potential multifunction activities of Cefixime@Hematite nanosystem. *Surface. Interfac.* 30, 101877 <https://doi.org/10.1016/j.surf.2022.101877>.
- Al-Jlil, S., 2017. Performance of nano-filtration and reverse osmosis processes for wastewater treatment. *Mater. Tehnol.* 51, 541–548. <https://doi.org/10.17222/mit.2015.250>.
- Ayati, N., Saiyarsarai, P., Nikfar, S., 2020. Short and long term impacts of COVID-19 on the pharmaceutical sector. *DARU J Pharm Sci* 28, 799–805. <https://doi.org/10.1007/s40199-020-00358-5>.
- Ayawei, N., Ebelegi, A.N., Wankasi, D., 2017. Modelling and interpretation of adsorption isotherms. *J. Chem.* 2017, 1–11. <https://doi.org/10.1155/2017/3039817>.
- Azari, A., Malakoutian, M., Yaghmaein, K., Jaafarzadeh, N., Shariatifar, N., Mohammadi, G., Masoudi, M.R., Sadeghi, R., Hamzeh, S., Kamani, H., 2022. Magnetic NH₂-MIL-101(Al)/Chitosan nanocomposite as a novel adsorbent for the removal of azithromycin: modeling and process optimization. *Sci. Rep.* 12, 18990 <https://doi.org/10.1038/s41598-022-21551-3>.
- Baresel, C., Harding, M., Fång, J., 2019. Ultrafiltration/granulated active carbon-biofilter: efficient removal of a broad range of micropollutants. *Appl. Sci.* 9, 710. <https://doi.org/10.3390/app9040710>.
- Bukalo, N.N., Ekosse, G.-I.E., Odiyo, J.O., Ogola, J.S., 2017. Fourier transform infrared spectroscopy of clay size fraction of cretaceous-tertiary kaolins in the douala sub-basin, Cameroon. *Open Geosci.* 9 <https://doi.org/10.1515/geo-2017-0031>.
- Caban, M., Stepnowski, P., 2021. How to decrease pharmaceuticals in the environment? A review. *Environ. Chem. Lett.* 19, 3115–3138. <https://doi.org/10.1007/s10311-021-01194-y>.
- Cerepi, A., Burlot, R., Galaup, S., Barde, J.-P., Loisy, C., Humbert, L., 2002. Effects of porous solid structures on the electrical behaviour: prediction key of transport properties in sedimentary reservoir rock. In: *Studies in Surface Science and Catalysis*. Elsevier, pp. 483–490. [https://doi.org/10.1016/S0167-2991\(02\)80171-9](https://doi.org/10.1016/S0167-2991(02)80171-9).
- Chandrasekhar, S., Ramaswamy, S., 2002. Influence of mineral impurities on the properties of kaolin and its thermally treated products. *Appl. Clay Sci.* 21, 133–142. [https://doi.org/10.1016/S0169-1317\(01\)00083-7](https://doi.org/10.1016/S0169-1317(01)00083-7).
- Chauhan, M., Saini, V.K., Suthar, S., 2020a. Removal of pharmaceuticals and personal care products (PPCPs) from water by adsorption on aluminum pillared clay. *J. Porous Mater.* 27, 383–393. <https://doi.org/10.1007/s10934-019-00817-8>.
- Chauhan, M., Saini, V.K., Suthar, S., 2020b. Ti-pillared montmorillonite clay for adsorptive removal of amoxicillin, imipramine, diclofenac-sodium, and paracetamol from water. *J. Hazard Mater.* 399, 122832 <https://doi.org/10.1016/j.jhazmat.2020.122832>.
- Corbin, G., Vuilliet, E., Lanson, B., Rimola, A., Mignon, P., 2021. Adsorption of pharmaceuticals onto smectite clay minerals: a combined experimental and theoretical study. *Minerals* 11, 62. <https://doi.org/10.3390/min11010062>.
- Cundari, L., Sari, K.F., Anggraini, L., 2018. Batch study, kinetic and equilibrium isotherms studies of dye adsorption of jumputan wastewater onto betel nuts adsorbent. *J. Phys.: Conf. Ser.* 1095, 012018 <https://doi.org/10.1088/1742-6596/1095/1/012018>.
- de Franco, M.A.E., de Carvalho, C.B., Bonetto, M.M., de Pellegrini Soares, R., Fêris, L.A., 2018. Diclofenac removal from water by adsorption using activated carbon in batch mode and fixed-bed column: isotherms, thermodynamic study and breakthrough curves modeling. *J. Clean. Prod.* 181, 145–154. <https://doi.org/10.1016/j.jclepro.2018.01.138>.
- Elamin, M.R., Abdulkhair, B.Y., Algethami, F.K., Khezami, L., 2021. Linear and nonlinear investigations for the adsorption of paracetamol and metformin from water on acid-treated clay. *Sci. Rep.* 11, 13606 <https://doi.org/10.1038/s41598-021-93040-y>.
- Ewis, D., Ba-Abbad, M.M., Benamor, A., El-Naas, M.H., 2022. Adsorption of organic water pollutants by clays and clay minerals composites: a comprehensive review. *Appl. Clay Sci.* 229, 106686 <https://doi.org/10.1016/j.clay.2022.106686>.
- Femina Carolin, C., Senthil Kumar, P., Janet Joshiba, G., Vinoth Kumar, V., 2021. Analysis and removal of pharmaceutical residues from wastewater using membrane bioreactors: a review. *Environ. Chem. Lett.* 19, 329–343. <https://doi.org/10.1007/s10311-020-01068-9>.
- Ferreira, R.C., De Lima, H.H.C., Cândido, A.A., Couto Junior, O.M., Arroyo, P.A., De Carvalho, K.Q., Gauze, G.F., Barros, M.A.S.D., 2015. Adsorption of paracetamol using activated carbon of dende and babassu coconut mesocarp. *International Journal of Biotechnology and Bioengineering* 9, 6. <https://doi.org/10.5281/zenodo.1106943>.
- García, R., Martínez-Ramírez, S., Frías, M., 2017. Effects of calcination temperature and the addition of ZnO on coal waste activation: a mineralogical and morphological evolution. *Appl. Clay Sci.* 150, 1–9. <https://doi.org/10.1016/j.clay.2017.08.031>.
- Giles, C.H., MacEwan, T.H., Nakhwa, S.N., Smith, D., 1960. Studies in adsorption. Part XI. A system of classification of solution adsorption isotherms, and its use in diagnosis of adsorption mechanisms and in measurement of specific surface areas of solids. *J. Chem. Soc.* 3973 <https://doi.org/10.1039/jr9600003973>.
- Han, R., Wang, Yu, Zhao, X., Wang, Yuanfeng, Xie, F., Cheng, J., Tang, M., 2009. Adsorption of methylene blue by phoenix tree leaf powder in a fixed-bed column: experiments and prediction of breakthrough curves. *Desalination* 245, 284–297. <https://doi.org/10.1016/j.desal.2008.07.013>.
- Hidayah, M., Kustomo, K., Yunita, A.I., 2023. Batch adsorption of Pb(II) batch using humic acid from goat dung. *Ark. Kemi* 9, 55–61. <https://doi.org/10.15575/ak.v9i2.19735>.
- Juela, D.M., 2020. Comparison of the adsorption capacity of acetaminophen on sugarcane bagasse and corn cob by dynamic simulation. *Sustain Environ Res* 30, 23. <https://doi.org/10.1186/s42834-020-00063-7>.
- Jyoti Sen, D., Patel, J.G., 2016. Logarithmic partition coefficient comparison study and molecular weight of synthesized prodrugs of Ibuprofen+Paracetamol, diclofenac Sodium+Paracetamol and Ibuprofen+Diclofenac sodium. *Am. J. Drug Deliv.* 4 <https://doi.org/10.21767/2321-547X.1000003>.
- Kamatichi, C., Arivoli, S., Prabakaran, R., 2022. Thermodynamic, kinetic, batch adsorption and isotherm models for the adsorption of nickel from an artificial solution using chloroxylon swietenia activated carbon. *Physical Chemistry Research* 10. <https://doi.org/10.22036/PCR.2021.300561.1956>.
- Kara, İ., Yilmazer, D., Akar, S.T., 2017. Metakaolin based geopolymer as an effective adsorbent for adsorption of zinc(II) and nickel(II) ions from aqueous solutions. *Appl. Clay Sci.* 139, 54–63. <https://doi.org/10.1016/j.clay.2017.01.008>.
- Kassa, A.E., Shibeshi, N.T., Tizazu, B.Z., 2022. Kinetic analysis of dehydroxylation of Ethiopian kaolinite during calcination. *J. Therm. Anal. Calorim.* 147, 12837–12853. <https://doi.org/10.1007/s10973-022-11452-y>.
- Kerkhoffs, C.M., Boit Martinello, K. da, Franco, D.S.P., Netto, M.S., Georjina, J., Foletto, E. L., Picilli, D.G.A., Silva, L.F.O., Dotto, G.L., 2021. Adsorption of ketoprofen and paracetamol and treatment of a synthetic mixture by novel porous carbon derived from *Butia capitata* endocarp. *J. Mol. Liq.* 339, 117184 <https://doi.org/10.1016/j.molliq.2021.117184>.
- Khazri, H., Ghorbel-Abid, I., Kalfat, R., Trabelsi-Ayadi, M., 2017. Removal of ibuprofen, naproxen and carbamazepine in aqueous solution onto natural clay: equilibrium, kinetics, and thermodynamic study. *Appl. Water Sci.* 7, 3031–3040. <https://doi.org/10.1007/s13201-016-0414-3>.
- Kryuchkova, M., Batasheva, S., Akhatova, F., Babaev, V., Buzyurova, D., Vikulina, A., Volodkin, D., Fakhruddin, R., Rozhina, E., 2021. Pharmaceuticals removal by adsorption with montmorillonite nanoclay. *IJMS* 22, 9670. <https://doi.org/10.3390/ijms22189670>.
- Kumari, N., Mohan, K., 2021. Basics of clay minerals and their characteristic properties. In: *Morari Do Nascimento, G. (Ed.), Clay and Clay Minerals*. IntechOpen. <https://doi.org/10.5772/intechopen.97672>.
- Lachaal, F., Mlayah, A., Anane, M., Bédir, M., Tarhouni, J., Leduc, C., 2013. Comprehension and hydrogeological conceptualization of aquifer in arid and semi-arid regions using integrated hydrogeological information system: case of the deep aquifer of Zéramdine-Béni Hassen (east-central Tunisia). *Arabian J. Geosci.* 6, 2655–2671. <https://doi.org/10.1007/s12517-011-0498-x>.
- Lechien, J.R., Chiesa-Estomba, C.M., De Siati, D.R., Horoi, M., Le Bon, S.D., Rodriguez, A., Dequanter, D., Blecic, S., El Afia, F., Distinguin, L., Chekkoury-Idrissi, Y., Hans, S., Delgado, I.L., Calvo-Henriquez, C., Lavigne, P., Falanga, C., Barillari, M.R., Cammaroto, G., Khalife, M., Leich, P., Souchay, C., Rossi, C., Journe, F., Hsieh, J., Edjlali, M., Carlier, R., Ris, L., Lovato, A., De Filippis, C., Coppee, F., Fakhry, N., Ayad, T., Saussez, S., 2020. Olfactory and gustatory dysfunctions as a clinical presentation of mild-to-moderate forms of the coronavirus disease (COVID-19): a multicenter European study. *Eur. Arch. Oto-Rhino-Laryngol.* 277, 2251–2261. <https://doi.org/10.1007/s00405-020-05965-1>.
- Lee, S., Yang, S., Lee, D., Choi, H., Won, J., 2023. Methylene blue transport in a sand-illite mixture and its implications for contaminant transport. *Hydrogeol. J.* <https://doi.org/10.1007/s10040-023-02647-0>.
- Lertcumfu, N., Jaita, P., Rujjanagul, G., Tunkasiri, T., 2018. Characterization of metakaolin-based materials for dye adsorption from aqueous solution. *SSP* 283, 88–94. <https://dx.doi.org/10.4028/www.scientific.net/SSP.283.88>.
- Li, T., Liu, Y., Peng, Q., Hu, X., Liao, T., Wang, H., Lu, M., 2021. Removal of lead(II) from aqueous solution with ethylenediamine-modified yeast biomass coated with magnetic chitosan microparticles: kinetic and equilibrium modeling. *Chem. Eng. J.* 214, 189–197. <https://doi.org/10.1016/j.cej.2012.10.055>.
- Liu, L., Liu, Q., Zhang, S., Li, Y., Yang, L., 2022. The thermal transformation behavior and products of pyrite during coal gangue combustion. *Fuel* 324, 124803. <https://doi.org/10.1016/j.fuel.2022.124803>.
- López-Cervantes, J., Sánchez-Machado, D.I., Sánchez-Duarte, R.G., Correa-Murrieta, M. A., 2018. Study of a fixed-bed column in the adsorption of an azo dye from an aqueous medium using a chitosan–glutaraldehyde biosorbent. *Adsorpt. Sci. Technol.* 36, 215–232. <https://doi.org/10.1177/0263617416688021>.
- Maalla, I., Boussen, Slim, Nathalie, F., Gaied, M.E., 2021. Incorporation of siliceous sand and lignite tailings from Miocene deposits (Zeramdine, Eastern Tunisia) in clay bricks and ceramic tiles: technological feasibility. *Arabian J. Geosci.* 14, 282. <https://doi.org/10.1007/s12517-021-06582-w>.
- Mabrouki, H., Akretche, D.E., 2016. Diclofenac potassium removal from water by adsorption on natural and pillared clay. *Desalination Water Treat.* 57, 6033–6043. <https://doi.org/10.1080/19443994.2014.1002008>.
- Maia, G., Andrade, J., Oliveira, M., Vieira, M.G.A., Silva, M.G.C., 2017. Affinity studies between drugs and clays as adsorbent. *Material. Chemical Engineering Transactions*. Mansouri, F., Chouchene, K., Roche, N., Ksibi, M., 2021. Removal of pharmaceuticals from water by adsorption and advanced oxidation processes: state of the art and trends. *Appl. Sci.* 11, 6659. <https://doi.org/10.3390/app11146659>.
- Mark, U., Anyakwo, C.N., Onyemaobi, O.O., Nwobodo, C.S., 2019. Conditions for thermal activation of ngwo clay as an alternative resource for alumina. *NR* 10, 1–15. <https://doi.org/10.4236/nr.2019.101001>.
- Mkaouar, S., Maherzi, W., Pizette, P., Zaitan, H., Benzina, M., 2019. A comparative study of natural Tunisian clay types in the formulation of compacted earth blocks. *J. Afr. Earth Sci.* 160, 103620 <https://doi.org/10.1016/j.jafrearsci.2019.103620>.
- Nguyen, P.Y., Carvalho, G., Reis, M.A.M., Oehmen, A., 2021. A review of the biotransformations of priority pharmaceuticals in biological wastewater treatment processes. *Water Res.* 188, 116446 <https://doi.org/10.1016/j.watres.2020.116446>.
- Nourmoradi, H., Moghadam, K.F., Jafari, A., Kamarehieh, B., 2018. Removal of acetaminophen and ibuprofen from aqueous solutions by activated carbon derived from *Quercus Brantii* (Oak) acorn as a low-cost biosorbent. *J. Environ. Chem. Eng.* 6, 6807–6815. <https://doi.org/10.1016/j.jece.2018.10.047>.
- Padmavathy, K.S., Madhu, G., Haseena, P.V., 2016. A study on effects of pH, adsorbent dosage, time, initial concentration and adsorption isotherm study for the removal of

- hexavalent chromium (Cr (VI)) from wastewater by magnetite nanoparticles. *Procedia Technology* 24, 585–594. <https://doi.org/10.1016/j.protcy.2016.05.127>.
- Park, J., Kim, C., Hong, Y., Lee, W., Chung, H., Jeong, D.-H., Kim, H., 2020. Distribution and removal of pharmaceuticals in liquid and solid phases in the unit processes of sewage treatment plants. *IJERPH* 17, 687. <https://doi.org/10.3390/ijerph17030687>.
- Quinn, H.M., 2014. A reconciliation of packed column permeability data: column permeability as a function of particle porosity. *J. Mater.* 2014, 1–22. <https://doi.org/10.1155/2014/636507>.
- Rafati, L., Ehrampoush, M.H., Rafati, A.A., Mokhtari, M., Mahvi, A.H., 2019. Fixed bed adsorption column studies and models for removal of ibuprofen from aqueous solution by strong adsorbent Nano-clay composite. *J Environ Health Sci Engineer* 17, 753–765. <https://doi.org/10.1007/s40201-019-00392-9>.
- Romdhani, M., Attia, A., Charcosset, C., Mahouche-Chergui, S., Ates, A., Duplay, J., Ben Amar, R., 2023. Optimization of paracetamol and chloramphenicol removal by novel activated carbon derived from sawdust using response surface methodology. *Sustainability* 15, 2516. <https://doi.org/10.3390/su15032516>.
- Salaa, F., 2021. *Intercalation d'une argile de type 1:1 par HDTMA et application à la coadsorption de produits pharmaceutiques (Thèse de Doctorat)*. Université Abdelhamid Ibn Badis Mostaganem, Algérie.
- Smiljanić, D., de Gennaro, B., Izzo, F., Langella, A., Daković, A., Germinario, C., Rottinghaus, G.E., Spasojević, M., Mercurio, M., 2020. Removal of emerging contaminants from water by zeolite-rich composites: a first approach aiming at diclofenac and ketoprofen. *Microporous Mesoporous Mater.* 298, 110057. <https://doi.org/10.1016/j.micromeso.2020.110057>.
- Sousa, M.U., Rodrigues, A.M., Araujo, M.E.B., Menezes, R.R., Neves, G.A., Lira, H.L., 2022. Adsorption of sodium diclofenac in functionalized palygoskite clays. *Materials* 15, 2708. <https://doi.org/10.3390/ma15082708>.
- Streit, A.F.M., Collazzo, G.C., Druzian, S.P., Verdi, R.S., Foletto, E.L., Oliveira, L.F.S., Dotto, G.L., 2021. Adsorption of ibuprofen, ketoprofen, and paracetamol onto activated carbon prepared from effluent treatment plant sludge of the beverage industry. *Chemosphere* 262, 128322. <https://doi.org/10.1016/j.chemosphere.2020.128322>.
- Sulaiman, S.M., Al-Jabari, M.H., 2021. Enhanced adsorptive removal of diclofenac sodium from aqueous solution by bentonite-supported nanoscale zero-valent iron. *Arab Journal of Basic and Applied Sciences* 28, 51–63. <https://doi.org/10.1080/25765299.2021.1878655>.
- Szabová, P., Varjúová, D., Kováčová, M., Prousek, J., Bodík, I., 2022. What is the effect of changing pH on pharmaceuticals' sorption? *Pol. J. Environ. Stud.* 31, 1805–1812. <https://doi.org/10.15244/pjoes/142580>.
- Tatarchuk, T., Soltys, L., Macyk, W., 2023. Magnetic adsorbents for removal of pharmaceuticals: a review of adsorption properties. *J. Mol. Liq.* 384, 122174. <https://doi.org/10.1016/j.molliq.2023.122174>.
- Thiebault, T., Boussafir, M., Fougère, L., Destandau, E., Monnin, L., Le Milbeau, C., 2019. Clay minerals for the removal of pharmaceuticals: initial investigations of their adsorption properties in real wastewater effluents. *Environ. Nanotechnol. Monit. Manag.* 12, 100266. <https://doi.org/10.1016/j.enmm.2019.100266>.
- Tironi, A., Trezza, M.A., Irassar, E.F., Scian, A.N., 2012. Thermal treatment of kaolin: effect on the pozzolanic activity. *Procedia Materials Science* 1, 343–350. <https://doi.org/10.1016/j.mspro.2012.06.046>.
- Wahyuni, N., Gusrizal, Juliawati, Y., 2023. Calcined kaolin as adsorbent for organic compounds in peat water. In: Doyan, A., Hadisaputra, S., Kechik, M.M.A., Bilad, M. R., Wei, C.-M., Susilawati (Eds.), *Proceedings of the 2nd International Conference on Science Education and Sciences 2022 (ICESSES 2022)*, Advances in Physics Research. Atlantis Press International BV, Dordrecht, pp. 263–271. https://doi.org/10.2991/978-94-6463-232-3_27.
- Wang, J., Guo, X., 2020. Adsorption isotherm models: classification, physical meaning, application and solving method. *Chemosphere* 258, 127279. <https://doi.org/10.1016/j.chemosphere.2020.127279>.
- Yanyan, L., Kurniawan, T.A., Zhu, M., Ouyang, T., Avtar, R., Dzarfan Othman, M.H., Mohammad, B.T., Albadarin, A.B., 2018. Removal of acetaminophen from synthetic wastewater in a fixed-bed column adsorption using low-cost coconut shell waste pretreated with NaOH, HNO₃, ozone, and/or chitosan. *J. Environ. Manag.* 226, 365–376. <https://doi.org/10.1016/j.jenvman.2018.08.032>.
- Yukselen, Y., Kaya, A., 2003. Zeta potential of kaolinite in the presence of alkali, alkaline earth and hydrolyzable metal ions. *Water Air Soil Pollut.* 155–168. <https://doi.org/10.1023/A:1023684213383>.